Chemistry & Biology, Vol. 9, 915–924, August, 2002, ©2002 Elsevier Science Ltd. All rights reserved. PII S1074-5521(02)00186-2

Structure-Activity Analysis of the Purine Binding Site of Human Liver Glycogen Phosphorylase

Jennifer L. Ekstrom,[1,7] Thomas A. Pauly,[1] Maynard D. Carty,[2] Walter C. Soeller,[2] Jeff Culp,[1] Dennis E. Danley,[1] Dennis J. Hoover,[3] Judith L. Treadway,[2] E. Michael Gibbs,[2] Robert J. Fletterick,[7] Yasmina S.N. Day,[4] David G. Myszka,[4] and Virginia L. Rath[1,5,6]

[1]Exploratory Medicinal Sciences
[2]Department of Cardiovascular and Metabolic Diseases Biology
[3]Medicinal Chemistry
Groton Laboratories
Pfizer Global Research and Development
Groton, Connecticut 06340
[4]Center for Biomolecular Interaction Analysis
University of Utah
School of Medicine
Salt Lake City, Utah 81432

Summary

Human liver glycogen phosphorylase (HLGP) catalyzes the breakdown of glycogen to maintain serum glucose levels and is a therapeutic target for diabetes. HLGP is regulated by multiple interacting allosteric sites, each of which is a potential drug binding site. We used surface plasmon resonance (SPR) to screen for compounds that bind to the purine allosteric inhibitor site. We determined the affinities of a series of compounds and solved the crystal structures of three representative ligands with K_D values from 17–550 μM. The crystal structures reveal that the affinities are partly determined by ligand-specific water-mediated hydrogen bonds and side chain movements. These effects could not be predicted; both crystallographic and SPR studies were required to understand the important features of binding and together provide a basis for the design of new allosteric inhibitors targeting this site.

Introduction

In the United States, 8 million people have been diagnosed (a similar number are estimated to be affected but undiagnosed) with type 2 diabetes mellitus, a disease characterized by high serum glucose levels and complications that include nerve and kidney damage, blindness, premature atherosclerosis, and heart disease [1]. The metabolic basis of the disease is not well understood but consists of both resistance to insulin action and defects in pancreatic insulin secretion. Exacting control of plasma glucose levels significantly reduces the extent and progression of complications but is difficult to achieve using current therapies [2]. Safer and more effective avenues for treatment are urgently needed. Liver glycogen phosphorylase controls the release of glucose-1-phosphate from liver glycogen stores and plays a central role in hepatic glucose output. In diabetic patients, release of glucose from the liver is inappropriately regulated and remains high when production is normally shut off (such as after a meal, when digestion raises blood glucose levels), suggesting that inhibitors of human liver glycogen phosphorylase may be useful in treating diabetes. Studies have shown that serum glucose levels can be lowered significantly by the inhibition of HLGP in a mouse model of diabetes [3, 4].

Typically, drug-development efforts have focused on compounds that bind at the *catalytic* sites of enzymes, but here we consider the possibility of *allosteric* inhibitors, several of which have been recently described [5]. HLGP is a highly regulated allosteric enzyme that switches between activated and inactivated forms depending on the phosphorylation state of the enzyme and the presence of allosteric activators and inhibitors that bind to multiple, distinct loci. In theory, each of the allosteric sites on HLGP could be a potential drug binding site. Known allosteric inhibitors of this enzyme include Bayer W1807, which localizes to the nucleotide binding site [6, 7], and sugar derivatives that are found at the glucose inhibitor site [8]. In addition, a novel (perhaps nonphysiological) binding site, termed the indole inhibitor site, was identified crystallographically in HLGP using a series of compounds synthesized at Pfizer [9, 10].

To develop screening methods specific for ligands which bind at the allosteric effector sites, we used the purine inhibitor site of HLGP, which is known to act synergistically with glucose. This synergism is a result of the proximity of the purine and glucose binding sites to each other and to the catalytic site. Both glucose and purines inhibit HLGP by stabilizing the inactive conformation of the enzyme, in which substrates are prevented from entering the catalytic site. Glucose dependency could be a useful property in an HLGP inhibitor intended for diabetic patients. A drug that provides reduced inhibition when glucose levels are low and increased inhibition in the presence of elevated glucose levels could reduce the risk of dangerous hypoglycemic episodes while still retaining efficacy when needed.

Using surface plasmon resonance technology, we measured binding affinities of commercially available compounds expected to bind at the purine site. These compounds are expected to function kinetically as allosteric inhibitors. The SPR assay was reliable and extremely sensitive, enabling the detection of small molecules to a protein 500-fold greater in mass. In addition, binding of small molecules to *inactive* states of the enzyme were measured, information which may be important for understanding the longevity and distribution of the drug in vivo.

Subsequent to the SPR studies, we determined the crystal structures of HLGP complexed with three different purine site compounds (one flavin and two purines;

[5]Correspondence: virginia@thiospharm.com
[6]Current address: Thios Pharmaceuticals, Inc., 747 Fifty Second Street, Oakland, California 94609.
[7]Current address: Department of Biochemistry and Biophysics, University of California, San Francisco, California 94143.

Table 1. Crystal, Data Collection, and Refinement Statistics for the HLGP*a* and HLGP*b* Complexes Described

	HLGP*a*/caffeine[a], CP-403700, GlcNAc	HLGP*a*/uric acid, CP-403700, GlcNAc	HLGP*a*/riboflavin, CP-403700, GlcNAc	HLGP*b*/caffeine[a], CP-403700, GlcNAc
Data Collection/Scaling				
Space group	P3(1)	P3(1)	P3(1)	P3(1)
Cell dimensions	a = 124.7 Å b = 124.7 Å c = 124.5 Å	a = 124.0 Å b = 124.0 Å c = 123.3 Å	a = 124.4 Å b = 124.4 Å c = 124.0 Å	a = 124.1 Å b = 124.1 Å c = 123.8 Å
Resolution	99–2.1 Å	99–2.1 Å	99–2.1 Å	35–2.3 Å
Reflections	183,471	243,830	368,381	261,069
Unique	113,786	117,831	122,788	92,608
Redundancy	1.6	2.0	2.9	2.8
Completeness (%)	90.0 (60.3)	94.9 (75.5)	98.1 (95.3)	99.2 (97.3)
Rsym (%)	6.6 (47.5)	7.0 (41.7)	9.2 (41.8)	8.9 (41.3)
I/σ	9.4 (1.4)	9.6 (1.7)	11.4 (2.6)	11.8 (2.7)
Structural Refinement				
Resolution	50–2.25 Å	75–2.1 Å	99–2.1 Å	35–2.3 Å
R_{factor}	0.214	0.191	0.247	0.206
R_{free}	0.243	0.235	0.283	0.253
Number of non-H atoms				
Protein	12,837	12,858	12,840	12,882
Ligand	176	184	190	186
Water	602	779	539	466
B-factors (Å^2)				
Protein	30.6	31.9	35.8	36.7
All ligands	26.5	27.2	34.5	32.8
Purine-site ligand	33.0	53.2	62.6[b]	37.7
Waters	28.0	33.5	32.3	35.3
Rms deviations				
Bonds (Å)	0.006	0.010	0.009	0.007
Angles (°)	1.2	1.5	1.4	1.3
Dihedrals (°)	21.1	21.8	21.3	20.9

Numbers in parentheses give the statistics for the highest resolution bin.

[a] The two caffeine-bound structures include four caffeine molecules, two at the purine site and two additional caffeine molecules bound on the protein surface near Trp174. It is unlikely that this secondary site is biologically relevant, as it is removed from the dimer interface and positioned on the surface of the protein, rather than in a pocket. The structures with uric acid and riboflavin show no compound electron density at this second binding location.

[b] Riboflavin is considerably less well ordered in the second subunit. (B value for subunit 1, 50.4; B value for subunit 2, 75.4.)

Table 1) whose affinities ranged from 17 μM to 550 μM. The differences in affinities are not explained by the chemical structures of the inhibitors but can be rationalized in light of the crystallographic data. Optimal binding of the flavin compound is achieved by maximizing the hydrophobic contact to the protein. The smaller purine compounds compensate for their reduced hydrophobic surface area through the formation of stabilizing hydrogen bonds with ordered water molecules. The crystal structures show that although all three ligands stack between the phenylalanine and tyrosine side chains that comprise the site, each adopts a unique orientation within that constraint. Each specific orientation is stabilized by hydrogen bonds to water molecules whose locations are specified by the ligand. Because of these and other changes to the binding site, a crystallographic analysis was essential to identify the key interactions.

Results and Discussion

Validation of Biosensor Method

Purified HLGP*a* (phosphorylated at serine 14) or *b* (unphosphorylated) was coupled to a CM5 BIACORE biosensor chip via free amine groups using standard immobilization chemistry. To demonstrate that all effector sites were accessible and that the protein could undergo the conformational changes required for activity *in the chip environment*, we assayed the ability of HLGP to bind known ligands. Here, we present data for two inhibitor binding sites, the purine site and the glucose binding site.

The SPR method was first validated by measuring the interaction between HLGP*a* and a purine site ligand, caffeine. The raw biosensor data (Figure 1A) are displayed as a series of plots, termed sensorgrams, of response units (RUs) measured over time for different concentrations of caffeine. The number of RUs (*y* axis) is a measure of the change in refractive index at the chip surface on ligand binding and is proportional to the mass of the ligand bound to the protein. The assays were done in triplicate; the superposition of the sensorgram plots (Figure 1A) shows the sensitivity of the method and that the data are reproducible even for low RU values. The plot shows a sharp upward increase in RUs on first injection of the ligand, indicating that the binding reaction rapidly reaches equilibrium. Similarly, when the ligand is no longer present in the sample flowing over the chip, the RU values drop precipitously,

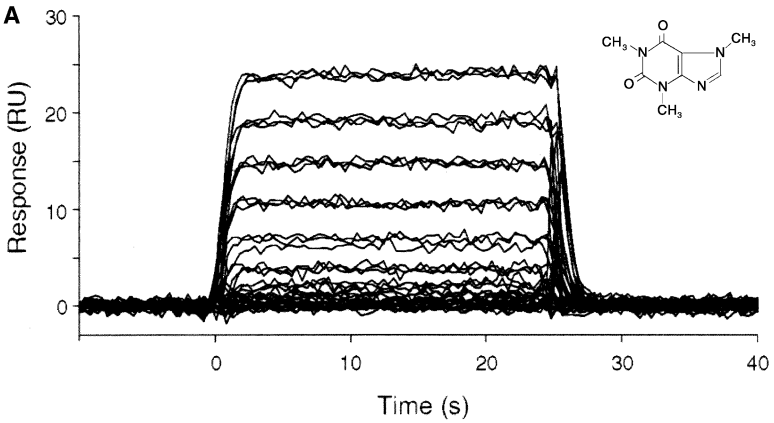

Figure 1. SPR Analysis of the Caffeine/HLGP*a* Interactions

(A) Binding responses were measured for caffeine (500 μM–2 μM by 2-fold dilutions) injected over a surface to which 21,000 RU HLGP*a* had been coupled.

(B) Equilibrium analysis of the caffeine/HLGP*a* interaction. Equilibrium binding responses for caffeine in the absence (filled squares) and presence (filled circles) of 50 mM glucose were independently fit to a 1:1 interaction model (solid lines) to determine equilibrium dissociation constants.

signaling that dissociation is also very fast. The raw sensorgram suggests that the interaction is relatively weak.

To extract out equilibrium binding constants, the sensorgram data can be combined and replotted as RU values at equilibrium versus ligand concentration (Figures 1B and 2). The data points may then be fitted to a model describing the nature of the interaction. In this case, a single affinity model, shown by the curve drawn through the individual data points, provides an excellent fit to the data. Based on the quality of the fit and its reproducibility (chips coupled with 10–20,000 RU; our unpublished data), more complicated models, such as mass transport limited, were not considered [11]. We

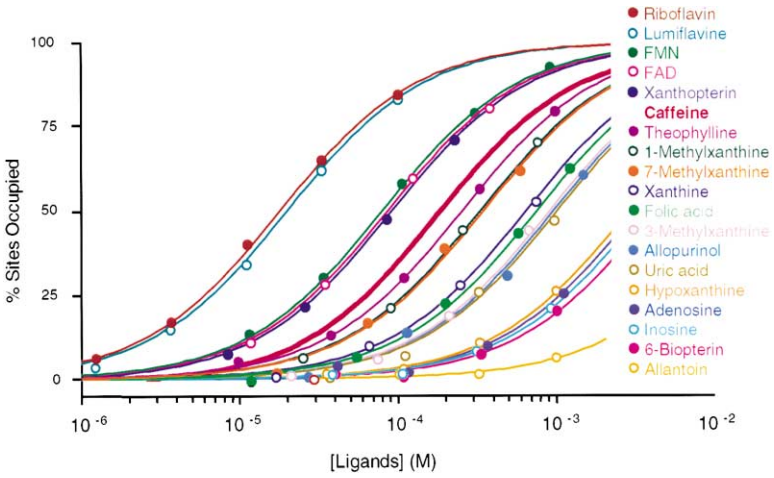

Figure 2. Purine Site Screen

For each of the 18 compounds tested, the RU values at equilibrium versus ligand concentration were fitted to a 1:1 interaction model. The resulting fitted curves are superimposed and listed in order on the right starting from the curve closest to the upper left (riboflavin) to the curve closest to the lower right (allantoin), with the labels color coded to match their respective binding isotherms. For clarity, only the curves for riboflavin, caffeine, and uric acid are labeled directly.

Table 2. Properties and SPR-Determined K_Ds of Purine Site Ligands

	Solvent-Accessible Surface Area (Å^2)	Percentage of Ligand Buried in Crystal Structure	Mass (Da)	No. of Rotatable Bonds	No. of Hydrogen-Bonding Groups	HLGP*a* K_D (μM)[a]	HLGP*b* K_D (μM)[a]
Riboflavin	581	55%	376.37	11	9	17	15
Lumiflavine	431		256.26	3	5	20	18
FMN	677		456.30	14	12	70	50
FAD	1,054		785.56	24	23	80	70
Xanthopterin	305		179.14	1	7	85	69
Caffeine	382	65%	194.19	3	3	108	92
Theophylline	346		180.17	2	4	150	120
1-methylxanthine	301		166.10	1	5	250	210
7-methylxanthine	314		166.10	1	5	280	260
Xanthine	293		152.11	0	6	320	290
Folic acid	689		441.40	11	13	380	470
3-methylxanthine	301		166.10	1	5	390	330
Allopurinol	260		136.11	1	5	420	370
Uric acid	399	53%	168.11	0	7	550	510
Hypoxanthine	273		136.11	0	5	1,220	1,130
Adenosine	451		267.24	6	9	1,370	1,310
Inosine	429		268.23	6	9	1,670	1,530
6-biopterin	421		237.22	6	8	1,770	1,750
Allantoin	278		158.12	3	7	7,960	9,560

[a] Each measurement is the average of duplicate experiments. The errors from duplicate measurements averaged 15% for the entire dataset.

assume that the biologically relevant symmetrical dimer binds two molecules of caffeine, as there is no evidence for half-site reactivity for any of the ligands that bind to HLGP. The midpoint of the curve gives the value for the affinity constant, K_D, of HLGP*a* for caffeine (108 +/− 10 μM). The error was determined experimentally by the average of five separate experiments. These results show that the biosensor assay is sufficiently sensitive to distinguish binding of a small molecule to a partner 500-fold greater in mass (194 Da compared to 100,000 Da).

Previous studies of glycogen phosphorylase from rabbit muscle [12] and rat liver [13] have shown that inhibition by glucose and caffeine is synergistic. To confirm that the HLGP*a* was in a biologically relevant state on the biosensor chip, we measured the effect of glucose on the enzyme's affinity for caffeine. We were able to observe glucose synergism by measuring the signal for caffeine in the presence and absence of 50 mM glucose (Figure 1B). Analysis of the biosensor data revealed the expected 2-fold difference in the K_Ds for caffeine: 108 μM without glucose and 65 μM with 50 mM glucose. The observed synergistic effects of caffeine and glucose indicate that HLGP functions as expected on the dextran chip surface.

We compared the affinities determined from the biosensor assay with data reported in the literature. The K_i for caffeine binding to rabbit muscle glycogen phosphorylase *a* (RMGP*a*) is 100 μM [12]; the K_D for caffeine binding to HLGP*a* measured on the biosensor is 108 μM. Thus, the results obtained using a strict binding assay on the biosensor are in the same range as those obtained from a kinetic analysis. The correspondence between binding and enzymatic data strongly suggests that the affinities measured using the biosensor represent a biologically relevant state of the enzyme in solution. This correspondence occurs despite important experimental differences (temperature, buffer, presence of activating substrates, and enzyme source) between our results and those reported in the literature.

Screen of the Purine Inhibitor Site

We used the biosensor to evaluate the affinities of a series of ligands expected to bind at the purine site, which had been previously assayed kinetically [14]. A similar protocol could be used to target any one of the allosteric loci. The biosensor chip contains four separate channels, permitting the screening of up to three different protein samples side by side, with the fourth channel serving as a reference. In this experiment, we used two channels for reference measurements and attached a sample of the phosphorylated and unphosphorylated forms of human liver glycogen phosphorylase to the other two channels. We tested 18 commercially available compounds (Table 2) and identified compounds that bound with both higher and lower affinities than caffeine. Riboflavin bound to HLGP*a* with the highest affinity (K_D = 17 μM), and allantoin bound with the weakest affinity (K_D = 7.9 mM), spanning a 470-fold difference in binding constants.

Under these conditions, the affinities of the 18 compounds for the HLGP*a* and HLGP*b* forms of the enzyme are of the same order of magnitude (Table 2). In theory, an allosteric inhibitor should have a higher affinity for the *inactive* form of the enzyme (HLGP*b*) than the active form (HLGP*a*). Such a change in ligand affinity is interpreted as a displacement of the inactive to active conformation equilibrium of the enzyme [15]. These affinities are usually measured by kinetic assays; for example, AMP has a higher affinity for the active conformation (K_D = 2 μM; [16, 17]) than the inactive conformation (K_D = 200 μM; [18]). We do not observe an affinity difference of this scale in the SPR assay, most likely because for HLGP the effect is not visible in the absence of substrates. We observe the same result testing other ligands one at a time in the SPR assay; the affinities for AMP, glucose, or glucose analogs for HLGP*a* and HLGP*b* are within the same order of magnitude, demonstrating that the effect is not specific to the purine site (our unpublished data). We note that the strength of the SPR assay described here is that it allows us to measure binding of

low affinity, low molecular mass compounds to specific sites on a 200 kDa enzyme. Rigorous confirmation that the ligands binding to the purine site function kinetically as allosteric inhibitors of HLGP requires a further analysis showing synergy with other ligands which stabilize the inactive conformation (e.g., glucose) and that binding of the inhibitor accelerates dephosphorylation of the enzyme (as has been done for the indole inhibitor site [9]). It is possible to develop an SPR screen that includes substrates; however, analysis of these results may be more complicated.

Compound Analysis

We calculated the hydrogen bonding potential, number of rotatable bonds, mass, and solvent-accessible surface area for each compound and looked for correlations between these properties and the binding affinities. Within the range of binding affinities observed, no correlations could be established.

Structures of HLGP*a*/Purine Site Ligand Complexes

To understand the structural details responsible for the measured differences in affinities at the purine site, we determined the X-ray crystal structures of three ligand complexes that span a 30-fold range in affinity: uric acid, caffeine, and riboflavin. Each purine site ligand was cocrystallized with HLGP*a* and two additional inhibitors that aided crystallization, presumably by stabilizing the protein conformation (N-acetyl-β-D-glucopyranosylamine, which binds at the glucose inhibitor site [19], and (S)-1-{2-[(5-chloro-1H-indole-2-carbonyl)-amino]-3-phenyl-propionyl}-azetidine-3-carboxylate (CP-403,700), which binds at the indole inhibitor site [9]). In addition to the structures solved, allantoin, the weakest purine site ligand, was also tested in numerous cocrystallization and soaking experiments. Although excellent crystals were obtained, no density corresponding to the ligand could be identified in any of the electron density maps.

Description of the Purine Inhibitor Binding Site

Each HLGP monomer is composed of two nearly equal sized domains; the catalytic site lies between the two. Riboflavin, caffeine, and uric acid all bind at the purine inhibitor site, which lies at the domain interface, approximately 12 Å from the catalytic site on the enzyme surface. The purine site can be minimally described as a slot formed between two parallel aromatic side chains. The principal features are hydrophobic and electronic stacking interactions between the planar ligand and the aromatic side chains of Phe285 and Tyr613. In addition to the hydrophobic interactions, each compound forms a specific set of water-mediated hydrogen bonds to residues surrounding the purine binding site.

Of the three complexes, the compound with the lowest affinity for HLGP*a* is uric acid ($K_D = 550\ \mu M$). Uric acid (Figure 3A and Table 2) forms a strong ring-stacking interaction with the aromatic group of Phe285. Its position relative to the ring of Tyr613 is slightly offset so that the primary interaction is with the Cα and Cβ atoms of Tyr613, rather than with the phenyl ring. Uric acid is oriented in the binding site through hydrogen bonds with three ordered water molecules (Table 3) which link it to the side chains of residues Asn282 and Glu287 and to the protein backbone at residues 283, 610, 612, and 570. A direct hydrogen bond between the purine ring of uric acid and the side chain oxygen of Asn282 is also formed. The hydrophobic and hydrogen bonding interactions observed involve residues belonging to both the N- and C-terminal domains and likely serve to stabilize their relative orientations.

Uric acid has four potential hydrogen bonds that are unsatisfied, three of which are located on the five-membered ring of the purine moiety and are buried within the site. The absence of such interactions indicates that uric acid is not an optimal ligand for this site. The average crystallographic B value (which may be taken as a measure of the order of the ligand) of uric acid is 53.2. This value is about 2-fold higher than the average B value for caffeine, another ligand that binds to this site (Table 2), suggesting that uric acid is less well ordered by comparison, consistent with its weaker affinity.

HLGP*a* binds caffeine with 5-fold greater affinity than uric acid. Whereas uric acid interacts primarily with the aliphatic moiety of Tyr613, caffeine forms additional van der Waals contacts with both the aliphatic and phenyl groups of Tyr613. This is possible because the hydrophobic surface of caffeine is increased relative to uric acid by its three methyl groups (Table 2). Although no direct hydrogen bonds are made between caffeine and the protein, water-mediated interactions specify its orientation. Caffeine forms hydrogen bonds to two ordered water molecules that link it to the main chain of residues 283, 570, 573, and 610 and to the side chains of Glu382, Glu572, and Arg770 (Table 3 and Figure 3B). Compared to uric acid, the purine ring of caffeine adopts a different rotational position in the binding site, thereby optimizing the hydrogen-bonding network and avoiding steric overlaps of the 1, 3, and 7 methyl substituents. The hydrogen bonds formed to uric acid are not present in the caffeine complex due to the presence of the 1-methyl group of caffeine. Instead, hydrogen bonds are formed to caffeine's two carbonyl groups. In contrast to uric acid, there is only a single unsatisfied hydrogen-bonding partner in caffeine (N^9), which is solvent accessible.

Early low-resolution studies of rabbit muscle phosphorylase *a* (RMGP*a*) crystals soaked with purine site ligands revealed the location of the purine inhibitor site [20]. More recently, two high-resolution structures of RMGP complexed with caffeine and other inhibitors have been determined (Protein Data Bank ID codes 1C8L and 1GFZ [7]). Interestingly, the orientation of the caffeine purine ring in human liver glycogen phosphorylase is distinct from that reported for RMGP. A comparison of our HLGP*a*/caffeine structure and the two caffeine-bound RMGP structures shows very good overlap between the corresponding residues of the purine site and conservation of each of the waters we observe interacting with caffeine; yet the caffeine molecule in RMGP is flipped 180 degrees relative to the caffeine in our structure. The two different rotational positions offer the same number of hydrogen-bonding groups in similar locales. The electron density for our HLGP*a* complex clearly supports our chosen orientation (Figure 3B).

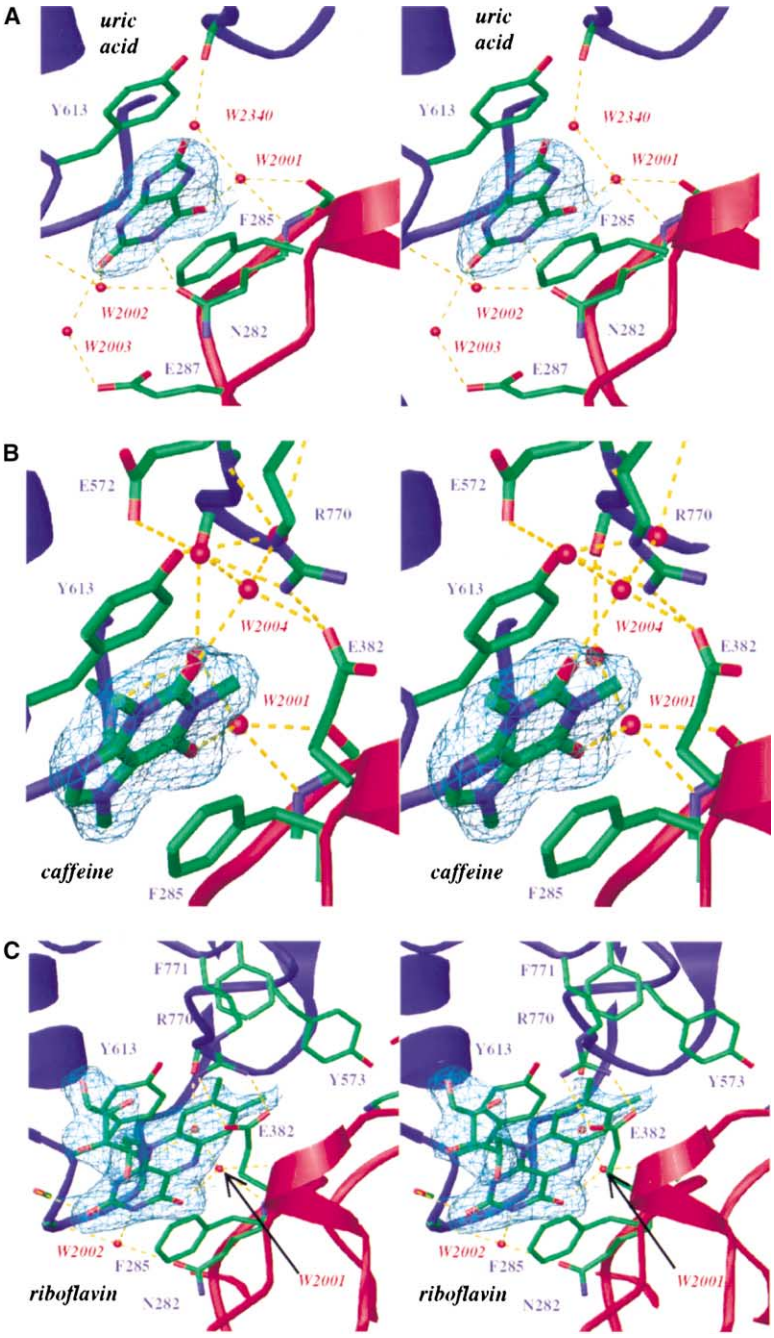

Figure 3. Crystal Structure of HLGP*a*/Purine Site Ligands

(A), Uric acid bound at the purine site; (B), caffeine bound at the purine site; (C), riboflavin bound at the purine site. The $2F_o$-F_c difference electron density for each ligand is contoured at 1σ above the mean. The figures were prepared using Ribbons [31], and each panel is colored as follows: structural elements of the N-terminal domain, red; those of the C-terminal domain, blue; oxygen atoms, red; nitrogen atoms, blue; carbon atoms, green; and water molecules are shown as red spheres.

Effect of Phosphorylation on Binding and Conformation

A comparison of the crystal structures of the phosphorylated and unphosphorylated enzymes complexed with caffeine, N-acetyl-β-D-glucopyranosylamine, and CP-403,700 confirms that the inactive conformation of the enzyme described here is independent of the phosphorylation state of the protein. The crystal structures of caffeine-bound HLGP*a* and caffeine-bound HLGP*b* look identical within error; the unphosphorylated N terminus is disordered in the HLGP*b* structure (as seen in the phosphorylated HLGP*a* structure), and no structural changes are transmitted to the purine or glucose inhibitory sites.

The purine site is preformed in the inactive conformation of human liver glycogen phosphorylase. The inactive conformation of HLGP*a* complexed with CP-403,700, a glucose analog, and caffeine may be compared with the structure of HLGP*a* complexed with the glucose analog alone (purine site empty). A comparison of the caffeine-bound and uric acid-bound structures with this inactive HLGP*a* [21] reveals that the positions of the phenyl groups of Phe285 and Tyr613 overlap well in all three structures. Thus, the binding of caffeine or uric acid does not create the binding site but serves to further stabilize an inactive conformation in which it already exists.

In contrast, the structure of HLGP*a* activated by AMP

Table 3. Key Interactions between Purine Site Ligands and HLGP

	Group 1	Group 2	Distance
HLGP*a*-uric acid	Uric O6	W 2001	2.4 Å
	Uric N1	Asn282 Oδ1	2.9 Å
	Uric O2	W 2003	3.0 Å
	Uric O2	W 2002	2.9 Å
	[a]Uric O6	Phe285 Cβ	3.2 Å
	Uric C5	Phe285 Cβ	3.3 Å
	Uric Cε2	Phe285 Cε2	3.5 Å
	Uric N7	Tyr613 Cδ2	3.4 Å
	Uric O8	Tyr613 Cζ	3.4 Å
	Uric C5	Tyr613 Cγ	3.6 Å
HLGP*a*-caffeine	Caffeine O6	W 2001	2.6 Å
	Caffeine O2	W 2004	2.6 Å
	[a]Caffeine O6	Phe285 Cβ	3.3 Å
	Caffeine C6	Phe285 Cγ	3.4 Å
	Caffeine N1	Phe285 Cδ1	3.5 Å
	Caffeine C6	Tyr613 Cγ	3.4 Å
	Caffeine C2	Tyr613 Cε1	3.4 Å
	Caffeine C1	Tyr613 Cε2	3.6 Å
HLGP*a*-riboflavin	Riboflavin O4	W 2001	2.6 Å
	Riboflavin N3	W 2002	2.9 Å
	[a]Riboflavin O4	Phe285 Cβ	3.2 Å
	Riboflavin C4	Phe285 Cγ	3.3 Å
	Riboflavin C4A	Phe285 Cδ1	3.3 Å
	Riboflavin C2	Tyr613 Cα	3.5 Å
	Riboflavin C5A	Tyr613 Cε2	3.5 Å
	Riboflavin C1	Tyr613 OH	3.5 Å
	Riboflavin C8	Glu382 Cγ	3.4 Å
	Riboflavin C8M	Glu382 Cδ	3.4 Å
	Riboflavin C7M	Tyr573 Cδ2	3.5 Å

[a] The three shortest atom to atom van der Waals contacts are given to facilitate comparison of the stacking interactions between each compound and the nearby Phe and Tyr rings.

[21] does not present a purine site capable of binding caffeine. The two C-terminal domains of the caffeine-bound inactive enzyme and the AMP-bound active conformation overlap well, placing Tyr613 in identical positions. However, in the active conformation, the loop containing Phe285 (the 280's loop) is displaced. Phe285 is moved 14 Å from its position in the caffeine-bound structure, displacing one wall of the slot observed in the inactive form. In agreement with this result, caffeine could not be soaked into or cocrystallized with the enzyme under the AMP complex crystallization conditions.

Binding of Flavins at the Caffeine Site

The highest affinity compound identified from our screen was riboflavin ($K_D = 17\ \mu M$; Table 2 and Figure 3C). The increased hydrophobic surface area of riboflavin relative to the two-ring systems of uric acid and caffeine allows more extensive contacts with the aliphatic and ring moieties of both Phe285 and Tyr613, contributing to improved binding. Several adjustments of the binding site are required to accommodate the larger ring system of riboflavin. Side chain movements result in an altered binding site, in which the hydrophobic interactions between riboflavin and the protein are optimized. In particular, the phenyl group of Phe285 is rotated around the chi1 dihedral approximately 1 Å toward the center of the flavin ring system, resulting in an improved stacking interaction. The chi3 dihedral angle of Glu382 is also altered to maximize packing of its side chain against the flavin ring. The salt bridge between Glu382 and Arg770 (Figure 3C) is optimized, such that both of its terminal oxygens are linked to one of the arginine terminal amino groups. Because both uric acid and caffeine lack the hydrophobic surface area required to pack against Glu382, no side chain rotation is seen, and only one terminal oxygen of Glu382 interacts with Arg770.

As in the complex with caffeine, no direct hydrogen bonds are formed between the protein and the riboflavin ligand. Water-mediated hydrogen bonds are formed between the flavin and backbone atoms of residues 283, 570, 610, and 612, as well as with the side chain of Asn282 (Table 3). The ribose moiety is partially disordered, but weak interactions (distances of 3.2 to 4.0 Å) can be observed between the ribose hydroxyls, two bound waters, and the side chains of Glu572 and Arg770. Riboflavin has one unsatisfied hydrogen bond at its N^5 position, which is not accessible to solvent.

The three crystal structures provide a basis for understanding the affinity constants for the purine analogs. Uric acid, the weakest binder, buries the least solvent-accessible surface area in the complex and exhibits high B values, suggesting some disorder in the bound conformation. Uric acid also suffers from unsatisfied hydrogen bonds at three positions oriented deep into the binding site as well as one oriented toward the bulk solvent. These unsatisfied hydrogen bonds may contribute to disorder and detract from the binding affinity. The 5-fold improved binding of caffeine relative to uric acid is consistent with the lower B values of caffeine and may be explained by improved hydrophobic interactions and a fully satisfied network of hydrogen bonds linking caffeine to the protein through water molecules. The 30-fold improved binding of riboflavin relative to uric acid can be attributed to the burying of a larger hydrophobic

surface area and to side chain movements that serve to optimize the interactions between the ligand and its binding site.

One potential high-affinity compound that we did not test is flavopiridol, a flavanoid that acts as an ATP-competitive inhibitor of cyclin-dependent kinases. Using kinetic rather than SPR assays, flavopiridol was shown to inhibit RMGP*a* and RMGP*b* with IC_{50}s of 2.5 μM and 1 μM, respectively. The structure of RMGP*b* with flavopiridol bound at the purine site has been determined [22]. Flavopiridol consists of three moieties: a central flavone 2-ring system, a piperidine, and a pendant 2-chlorophenyl group. Like riboflavin, the interactions of flavopiridol at the purine site are primarily hydrophobic (600 Å^2 of solvent accessible area buried, compare to 581 Å^2 for riboflavin). Flexibility in flavopiridol allows for optimized placement of the chlorine substituted phenyl group, which occupies roughly the same space as the hydrophobic end of the flavin ring in our HLGP*a*/riboflavin structure. The flavone ring does not overlap well with the flavin moiety of riboflavin, being 15° out of the plane and rotated 45° with respect to riboflavin. The piperidine ring fills a similar space as the riboflavin ribosyl group and is structurally more rigid but forms no contacts (neither direct nor water mediated) to surrounding residues of the protein. Flavopiridol forms hydrogen bonds to two ordered water molecules that correspond loosely to waters 2001 and 2002 observed in our riboflavin structure.

Role of Water Molecules

Crystallographically observed waters in the binding site likely play a critical role in determining the affinity of each ligand for HLGP. Only one of these buried waters (W2001) is conserved in all three structures. Caffeine, uric acid, and riboflavin all form hydrogen bonds with this buried water, yet each compound presents a different functional group for this interaction and positions itself in a distinct conformation within the binding site. This is of particular importance for the purine compounds, which, due to their smaller volume, assume different binding orientations depending on the nature of the attached functional groups.

Additional water molecules are recruited to satisfy potential hydrogen bonds. Their absence or presence is determined by steric conflicts and the ability to form hydrogen bonds with each purine site ligand. For example, uric acid recruits a water molecule (W2002) that is absent in the caffeine complex but present in the riboflavin complex where it forms a long hydrogen bond (3.4 Å) to riboflavin. This water is not observed in the caffeine structure, as it is displaced by caffeine's 7-methyl group. Uric acid also forms a hydrogen bond to W2003, which is not present in either of the other two complexes due to the lack of a nearby hydrogen-bonding partner in either caffeine or riboflavin. Caffeine also recruits a water molecule (W2004) that is not found in the other two structures either because of steric overlap (riboflavin) or because there is no hydrogen-bonding partner for it at that location (uric acid).

Conclusions

We have studied the binding of purine and flavin compounds to the human liver isozyme of glycogen phosphorylase. The flavin compounds exhibit the highest affinity, followed by purines, of which caffeine binds with the highest affinity. This set of binding and crystallographic data provides a basis from which allosteric effectors for the purine site could be developed.

The crystal structure shows that the flavin moiety derives its potency by interacting with only a fraction of the nearby hydrophobic surface. Side chain atoms of Glu382 and Tyr573 (and potentially others) are within van der Waals contact of the flavin C7 and C8 carbon positions; such interactions could be optimized. The fully conserved structural water (W2001) could be incorporated into the ligand through an extension off the flavin carbon C4. Although the flavin nitrogen N^5 likely participates in a hydrogen bond in solution, it does not in the complex; this feature could be exploited. Finally, charged residues Glu382, Glu572, and Arg770 are within hydrogen-bonding range of the ribose moiety; their proximity could be utilized. From these observations, we conclude that riboflavin, because it exploits only some of the potential interactions at this site, is not an optimal inhibitor. We also considered the possibility of linking the glucose and purine sites (which are only 10 Å apart) with a single compound; however, since the protein backbone (residues 283–285) occupies the region that lies between these two sites, it would prevent binding of any compound linking them. The crystallographic data shown here provide a basis for the design of more effective ligands for the purine site.

Flavopiridol and riboflavin are structurally distinct; however, the opportunities to improve the binding affinity of riboflavin may be equally applied to flavopiridol, with two exceptions. Flavopiridol already lacks the floppy ribose, having a piperidine instead, and also lacks the unsatisfied ring nitrogen of flavin. Taken together, these may account for its improved affinity to RMGP compared to riboflavin.

We have demonstrated that SPR technology is useful as a complement to crystallographic analyses of ligand binding. The SPR assay was sensitive enough to distinguish binding of small molecules to a partner 500-fold greater in mass and could likely be extended to a mass ratio of $>$1000. The SPR assays measure direct binding, are not dependent on enzyme activity, and could be used in a medium throughput mode; up to 200 compounds per day could be screened using current technologies. SPR binding assays can be used to screen for new allosteric inhibitors targeted to a particular effector locus by blocking all other binding sites with appropriate compounds.

Significance

Type 2 diabetes is a growing healthcare problem in the United States and throughout the world. The metabolic basis of the disease is complicated, involving both resistance to insulin action and defects in pancreatic insulin secretion, leading to devastating long-term complications such as atherosclerosis, blindness, and liver and kidney disease. Extended studies have shown that when blood glucose levels are maintained within the normal range, the extent and progression of com-

plications can be significantly reduced. However, such control is difficult to achieve using current therapies, and more effective treatments are needed. Human liver glycogen phosphorylase catalyzes the breakdown of liver glycogen stores to supply glucose for the blood; inhibition of glycogen phosphorylase results in lowered blood glucose in a mouse model of diabetes and thus presents a potential drug design target for diabetes.

Typically, drug development efforts have focused on the catalytic sites of enzymes, but here we consider the possibility of identifying allosteric inhibitors. HLGP is regulated by multiple interacting allosteric sites, each of which may be considered a potential drug binding locus. We used surface plasmon resonance methods to determine the affinities of a series of compounds that bind to the purine inhibitor site. Notably, the binding affinities did not track rationally with the chemical structures of the inhibitors. The crystal structures of three representative inhibitors complexed with the enzyme revealed the reasons for this: (1) the binding affinities are in part determined by ligand-specific water-mediated hydrogen bonds, (2) the ligands bind in different orientations within the pocket, and (3) side chains within the binding site are repositioned depending on the inhibitor bound. The combined binding and crystallographic data provide a basis for the design of new allosteric inhibitors targeting this site.

Experimental Procedures

Expression, Purification, and Crystallization

Phosphorylated human liver glycogen phosphorylase (HLGP*a*) was expressed in SF9 insect cells, purified, and assayed as described [9]. The unphosphorylated form (HLGP*b*) was prepared from *E. coli* cells, purified, and assayed as described [9]. Both the HLGP*a* and HLGP*b* preparations concluded with a Mono Q column chromatography step that efficiently separates the phosphorylated and unphosphorylated enzymes. In addition, activity assays were used to determine the relative amounts of HLGP*a* and HLGP*b* in each sample. In each case, the samples are estimated to have less than 10% of the contaminating phosphorylation state.

In preparation for crystallization, HLGP*a* was concentrated to 25–30 mg/ml in 20 mM NaBES (pH 6.8), 1 mM EDTA, and 0.5 mM dithiothreitol (DTT). After concentration, the allosteric effectors CP-403,700, N-acetyl-β-D-glucopyranosylamine, and either caffeine, uric acid, or riboflavin were added at concentrations of 0.1 mM, 0.1 mM, and 5 mM, respectively. Hanging drops were made with equal volumes of the protein complex and the reservoir solution (0.1 M NaMES [pH 6.0] and 25%–35% methylpentanediol [MPD]), and crystals were grown at 17°C.

The unphosphorylated HLGP*b* was concentrated to 15 mg/ml in 20 mM NaBES (pH 6.8), 1 mM EDTA, and 0.5 mM DTT. The allosteric effectors caffeine, CP-403,700, and N-acetyl-β-D-glucopyranosylamine were added at concentrations of 0.1 mM, 0.1 mM, and 5 mM, respectively. Hanging drops were made with equal volumes of protein and reservoir solution (0.1 M NaMES [pH 6.0] and 36%–40% MPD), and crystals were grown at 17°C.

Data Collection and Structure Solution

Prior to data collection, the HLGP*a* and HLGP*b* cocrystals were flash frozen in liquid nitrogen directly from the drop. The data for the HLGP*a* complexes were measured using a Brandeis B4 CCD detector [23] at beamline X12C, Brookhaven National Light Source; the data for the HLGP*b* complex were obtained at beamline 5.0.2 of the Advanced Light Source, Berkeley, CA. The data were processed using Denzo and Scalepack [24]. The structures were solved by molecular replacement using the published structure of the inactive HLGP*a* (Protein Data Bank ID code 1EXV) as a starting model. Refinement was carried out using iterative cycles of manual refitting in *O* [25] followed by refinement in CNS [26]. Ligand structures were generated and minimized using SYBYL (Tripos, Inc.) or PRODRG [27] and CNS. The crystal, data collection, and refinement statistics are given in Table 1.

Biosensor Assays

Surface plasmon resonance experiments were performed on a BIACORE 2000 instrument equipped with research grade CM5 sensor chips (BIAcore AB, Uppsala, Sweden). All HLGP surfaces were prepared at 35°C by an amine-coupling method [28] using reagents available from BIAcore AB (N-ethyl-N′-dimethylaminopropyl-carbodiimide [EDC], N-hydroxysuccinimide [NHS], and 1 M ethanolamine-HCl at pH 8.5). During the immobilization, the flow rate of the running buffer (50 mM HEPES [pH 7.2], 100 mM KCl, 2.5 mM EGTA, 2.5 mM $MgCl_2$, 1% dimethylsulfoxide [DMSO], 0.5 mM DTT) was 15 μL/min. Flow cells were activated for 6 min with a solution containing 50 mM NHS and 0.2 mM EDC. HLGP*a* and HLGP*b* were diluted to 0.1 mg/mL in 10 mM sodium phosphate (pH 5.0) and injected for 15 min. The remaining reactive groups were blocked with a 7 min injection of 1 M ethanolamine-HCl at pH 8.5. Typical immobilization levels of the HLGP proteins were between 20,000 and 30,000 RU. A nonderivatized flow cell served as a reference surface.

All small molecule binding data were collected at 20°C at a flow rate of 100 μL/min in a solution of running buffer (50 mM HEPES [pH 7.2], 100 mM KCl, 2.5 mM EGTA, 2.5 mM $MgCl_2$, 1% DMSO, 0.5 mM DTT) for both reference and reaction surfaces. Caffeine was dissolved directly in the running buffer at a stock concentration of 0.5 mM. For SPR analysis, 2-fold serial dilutions of stock caffeine solution were made in running buffer across the concentration series from 500 to 1.84 μM. Each concentration of caffeine was dispensed into three separate tubes and randomized in the sample racks. Samples were injected for 24 s using the KINJECT command followed by an injection of running buffer for 30 s. The injection flow cell was washed using the EXTRACLEAN command after each sample injection. An injection of running buffer (a "blank") was made after every fifth sample injection for the purpose of "double referencing" [29]. Five buffer solutions containing varying concentrations of DMSO (0.95%–1.1%) were injected to construct a calibration plot [30], which was used to correct for excluded volume differences between the reaction and reference surfaces. The entire caffeine binding experiment was repeated five times using new sensor chips and different preparations of HLGP*a* and HLGP*b* proteins as well as new caffeine stocks. Data for caffeine with 50 mM glucose added to the running buffer and samples were measured in the same way.

A set of ligands (adenosine, allantoin, allopurinol, 6-biopterin, caffeine, flavin adenine dinucleotide, flavin mononucleotide, folic acid, hypoxanthine, inosine, 1-methylxanthine, 3-methylxanthine, 7-methylxanthine, riboflavin, theophylline, uric acid, xanthine, and xanthopterin) was tested for binding to the HLGP surfaces using the procedure described above for caffeine, with the following alterations. Due to solubility concerns, each ligand was initially dissolved in pure DMSO; the DMSO stock solutions of each compound were then diluted in DMSO-free running buffer, giving a final DMSO content of 1% that matched the running buffer. Further dilutions were made serially in running buffer across a ligand concentration range from 1 to 0.001 mM. The entire screen was repeated twice using a newly prepared protein surface each time.

Biosensor Data Analysis

The raw response data were zeroed on both the response and time axes prior to the start of the injection. To correct for bulk refractive index changes, responses from a reference surface without protein were subtracted from the reaction surface data. In a second referencing step, the average of the responses from five buffer injections was used to correct for any systematic differences between flow cells [29]. To extract equilibrium dissociation constants, we plotted binding responses at equilibrium against ligand concentration and fit the data to a 1:1 interaction site model. Before fitting the data to the model, the response data from the screen were first normalized by dividing by the molecular mass of each compound. In the case of the purine site screen, the capacity of the chip was not saturated

for some weak affinity compounds (although binding reached equilibrium in all cases). To identify the saturation point for all compounds and to minimize the errors in the K_Ds, the equilibrium responses for all 18 compounds in the screen were fit simultaneously. Each measurement is the average of duplicate experiments; the errors from duplicate measurements averaged 15% for the entire dataset.

Acknowledgments

Thanks to Robert W. Sweet, Thomas Earnest, and Gerry McDermott for assistance during data collection.

Received: March 20, 2002
Revised: May 21, 2002
Accepted: June 17, 2002

References

1. DeFronzo, R.A. (1999). Pharmacologic therapy for type 2 diabetes mellitus. Ann. Int. Med. *131*, 281–303.
2. The Diabetes Control and Complications Trial Research Group. (1993). The effect of intensive treatment of diabetes on the development and progression of long-term complications in insulin-dependent diabetes mellitus. N. Engl. J. Med. *329*, 977–986.
3. Martin, W.H., Hoover, D.J., Armento, S.J., Stock, I.A., McPherson, R.K., Danley, D.E., Stevenson, R.W., Barrett, E.J., and Treadway, J.L. (1998). Discovery of a human liver glycogen phosphorylase inhibitor that lowers blood glucose *in vivo*. Proc. Natl. Acad. Sci. USA *95*, 1776–1781.
4. Fosgerau, F., Westergaard, N., Quistorff, B., Grunnet, N., Kristiansen, M., and Lundgren, K. (2000). Kinetic and functional characterization of 1,4-dideoxy-1,4-imino-D-arabinitol: a potent inhibitor of glycogen phosphorylase with anti-hyperglyceamic effect in ob/ob mice. Arch. Biochem. Biophys. *380*, 274–284.
5. DeDecker, B. (2000). Allosteric drugs: thinking outside the active-site box. Chem. Biol. *7*, R103–R107.
6. Oikanomakos, N.G., Titsanou, K.E., Zographos, S.E., Skamnaki, V.T., Goldmann, S., and Bischoff, H. (1999). Allosteric inhibition of glycogen phosphorylase *a* by the potential antidiabetic drug 3-isopropyl 4-(2-chlorophenyl)-1,4-dihydro-1-ethyl-2-methylpyridine-3,5,6-tricarboxylate. Protein Sci. *8*, 1930–1945.
7. Tsitsanou, K.E., Skamnaki, V.T., and Oikonomakos, N.G. (2000). Structural basis of the synergistic inhibition of glycogen phosphorylase *a* by caffeine and a potential antidiabetic drug. Arch. Biochem. Biophys. *384*, 245–254.
8. Gregoriou, M., Noble, M.E.M., Watson, K.A., Garman, E.F., Krulle, T.M., De La Fuente, C., Fleet, G.W.J., Oikonomakos, N.G., and Johnson, L.N. (1998). The structure of a glycogen phosphorylase glucopyranose spirohydantoin complex at 1. 8 Å resolution and 100 K: the role of the water structure and its contribution to binding. Protein Sci. *7*, 915–927.
9. Rath, V.L., Ammirati, M., Danley, D.E., Ekstrom, J.L., Gibbs, E.M., Hynes, T.R., Mathiowetz, A.M., McPherson, R.K., Olson, T.V., Treadway, J.L., et al. (2000). Human liver glycogen phosphorylase inhibitors bind at a new allosteric site. Chem. Biol. *7*, 677–682.
10. Oikonomakos, N.G., Skamnaki, V.T., Tsitsanou, K.E., Gavalas, N.G., and Johnson, L.N. (2000). A new allosteric site in glycogen phosphorylase *b* as a target for drug interactions. Structure *8*, 575–584.
11. Myszka, D.G., Morton, T.A., Doyle, M.L., and Chaiken, I.M. (1997). Kinetic analysis of a protein antigen-antibody interaction limited by mass transport on an optical biosensor. Biophys. Chem. *64*, 127–137.
12. Kasvinsky, P.J., Shechosky, S., and Fletterick, R.J. (1978). Synergistic regulation of phosphorylase *a* by glucose and caffeine. J. Biol. Chem. *253*, 9102–9106.
13. Ercan-Fang, N., and Nuttall, F.Q. (1997). The effect of caffeine and caffeine analogs on rat liver phosphorylase *a* activity. J. Pharmacol. Exp. Ther. *280*, 1312–1318.
14. Kasvinsky, P.J., Madsen, N.B., Sygusch, J., and Fletterick, R.J. (1978). The regulation of glycogen phosphorylase *a* by nucleotide derivatives. Kinetic and X-ray crystallographic studies. J. Biol. Chem. *253*, 3343–3351.
15. Monod, J., Wyman, J., and Changeux, J.-P. (1965). On the nature of allosteric transitions: a possible model. J. Mol. Biol. *12*, 88.
16. Engers, H.D., Shechosky, S., and Madsen, N.B. (1970). Kinetic mechanism of phosphorylase *a*: initial velocity studies. Can. J. Biochem. *48*, 746–754.
17. Mateo, P.L., Baron, C., Lopez-Mayorga, O., Jimenez, J.S., and Cortijo, M. (1984). AMP and IMP binding to glycogen phosphorylase *b*. J. Biol. Chem. *259*, 9384–9389.
18. Griffiths, J.R., Dwek, R.A., and Radda, G.C.K. (1976). Conformational changes in glycogen phosphorylase studied with a spin label probe. Eur. J. Biochem. *61*, 237–242.
19. Oikonomakos, N.G., Kontou, M., Zographos, S.E., Watson, K.A., Johnson, L.N., Bichard, C.J.F., Fleet, G.W.J., and Acharya, K.R. (1995). *N*-acetyl-β-D-glucopyranosylamine: a potent T-state inhibitor of glycogen phosphorylase. A comparison with α-D-glucose. Protein Sci. *4*, 2469–2477.
20. Kasvinsky, P.J., Madsen, N.B., Fletterick, R.J., and Sygusch, J. (1978). X-ray crystallographic and kinetic studies of oligosaccharide binding to phosphorylase. J. Biol. Chem. *253*, 1290–1296.
21. Rath, V.L., Ammirati, M.L., Lemotte, P.K., Fennell, K.F., Mansour, M.N., Danley, D.E., Hynes, T.R., Schulte, G.K., Wasilko, D.J., and Pandit, J. (2000). Activation of human liver glycogen phosphorylase by altering the secondary structure and packing of the catalytic core. Mol. Cell *6*, 1–20.
22. Oikonomakos, N.G., Schnier, J.B., Zographos, S.E., Skamnaki, V.T., Tsitsanou, K.E., and Johnson, L.N. (2000). Flavopiridol inhibits glycogen phosphorylase by binding at the inhibitor site. J. Biol. Chem. *44*, 34566–34573.
23. Phillips, W.C. (2000). Multiple CCD detector for macromolecular X-ray crystallography. J. Appl. Crystallogr. *33*, 243–251.
24. Otwinowski, Z., and Minor, W. (1997). Processing of X-ray diffraction data collected in oscillation mode. Methods Enzymol. *276*, 307–326.
25. Jones, T.A., Zou, J.-Y., Cowan, S.W., and Kjeldgaard, M. (1991). Improved methods for building protein models in electron density maps and the location of errors in these models. Acta Crystallogr. A *47*, 110–119.
26. Brunger, A.T., Adams, P.D., Clore, G.M., DeLano, W.L., Gros, P., Grosse-Kunstleve, R.W., Jiang, J.-S., Kuszewski, J., Nilges, M., Pannu, N.S., et al. (1998). Crystallography and NMR System; a new software suite for macromolecular structure determination. Acta Crystallogr. *D54*, 905–921.
27. van Aalten, D.M.F., Bywater, R., Findlay, J.B.C., Hendlich, M., Hooft, R.W.W., and Vriend, G. (1996). PRODRG, a program for generating molecular topologies and unique molecular descriptors from coordinates of small molecules. J. Comput. Aided Mol. Des. *10*, 255–262.
28. Johnsson, B., Lofas, S., and Lindquist, G. (1991). Immobilization of proteins to a carboxymethyldextran-modified gold surface for biospecific interaction analysis in surface plasmon resonance detectors. Anal. Biochem. *198*, 268–277.
29. Myszka, D.G. (1999). Improving biosensor analyis. J. Mol. Recognit. *12*, 279–284.
30. Frostell-Karlsson, A., Remaeus, A., Roos, A., Andersson, K., Borg, P., Hamalainen, M., and Karlsson, R. (2000). Biosensor analysis of the interaction between immobilized human serum albumin and drug compounds for prediction of human serum albumin binding levels. J. Med. Chem. *43*, 1986–1992.
31. Carson, M. (1991). Ribbons 2.0. J. Appl. Crystallogr. *24*, 958–961.

Accession Numbers

The coordinates for the complexes of HLGP*a* with caffeine, riboflavin, or uric acid and for HLGP*b* with caffeine have been deposited in the Protein Data Bank under ID codes 1L5Q, 1L5R, 1L5S, and 1L7X, respectively.